ChemComm

Chemical Communications

## Accepted Manuscript

This article can be cited before page numbers have been issued, to do this please use: H. Nagakawa and T. Tatsuma, *Chem. Commun.*, 2025, DOI: 10.1039/D5CC04077A.




ROYAL SOCIETY OF CHEMISTRY

rsc.li/chemcomm

ChemComm

View Article Online
DOI: 10.1039/D5CC04077A

COMMUNICATION

# Morphology optimization of CdS-Pt photocatalyst by photoetching for hydrogen production with high quantum efficiency

Received 00th January 20xx,
Accepted 00th January 20xx

DOI: 10.1039/x0xx00000x

Haruki Nagakawa *[a,b,c] and Tetsu Tatsuma *[a]



**Morphology of CdS-Pt photocatalyst was optimized in terms of photocatalytic activity and stability through photoetching of CdS. This achieved high external quantum efficiency for hydrogen production in an alkaline solution containing a sacrificial electron donor.**

In order to develop practical semiconductor photocatalysts, the important factors are active wavelength range, external quantum efficiency (EQE) and stability. Regarding the wavelength range, a bandgap less than ~3.0 eV is required for utilization of visible light, and the conduction band minimum and valence band maximum should be positioned appropriately to drive target redox reactions. Achieving these involves careful selection of semiconductors,[1] band engineering[2] or adopting Z-scheme systems.[3] Regarding EQE, it can easily be improved by increasing the particle concentration if the photocatalyst particles are suspended in a solution, as far as their internal quantum efficiency (IQE) is sufficiently high. To achieve high IQE, it is essential to effectively separate photoexcited electrons and holes and efficiently transfer them to reactive species. Strategies for these may include utilizing differences in the work function between different crystal facets for improved charge separation and depositing co-catalysts onto the photocatalyst for enhanced charge separation and redox reactions.[4,5] In addition, particle size and morphology play critical roles. Smaller particles offer a larger reactive surface area and increase the probability of photoexcited carriers reaching the particle surface before deactivation. Conversely, larger particles are advantageous for charge separation, which is promoted by band bending in a well-developed space charge layer, and for utilization of well-developed crystal facets with ideal work function and reactivity. Bumpy or protruding particles provide some of the benefits of both small and large particles, and are expected to achieve optimized photocatalytic performances. Although this class of carbon nitride photocatalysts have been developed through thermal exfoliation[6] and acid-etching,[7] the particle morphologies change in a random manner, and high quantum efficiency has not yet been achieved.

In the present study, highly crystalline submicron-sized wurtzite CdS was used to perform photocatalytic hydrogen generation coupled with oxidation of lactic acid, isopropanol or α-cellulose. CdS has a bandgap suitable for visible light absorption and the position of the conduction band minimum suitable for reduction of water to hydrogen. However, CdS is prone to corrosion during photocatalytic reactions,[8] in particular on unstable crystal facets, when the removal of holes is slower than the consumption of excited electrons.[9] Here we take advantage of this photocorrosion to automatically optimize the morphology of CdS-Pt photocatalyst particles for the target reactions (Fig. 1). Under given photocatalytic reaction conditions, excess holes etch the particles, increasing the area of stable facets and shortening the hole transport distance. This

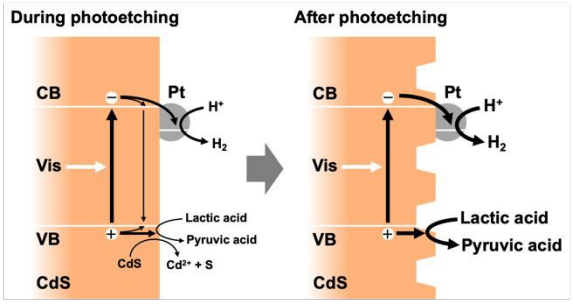


**Fig. 1** Schematic diagrams of the photocatalytic reactions before and after the photoetching.

[a] Institute of Industrial Science, The University of Tokyo, Tokyo 153-8505, Japan. E-mail: tatsuma@iis.u-tokyo.ac.jp
[b] Faculty of Applied Science and Engineering, Ibaraki University, Ibaraki 316-8511, Japan. E-mail: haruki.nagakawa.hb88@vc.ibaraki.ac.jp
[c] Carbon Recycling Energy Research Center, Ibaraki University, Ibaraki 316-8511, Japan.

Supplementary Information available: Details of some experimental methods, XRD data, DRS spectra XPS data, and cycling test. See DOI: 10.1039/x0xx00000x

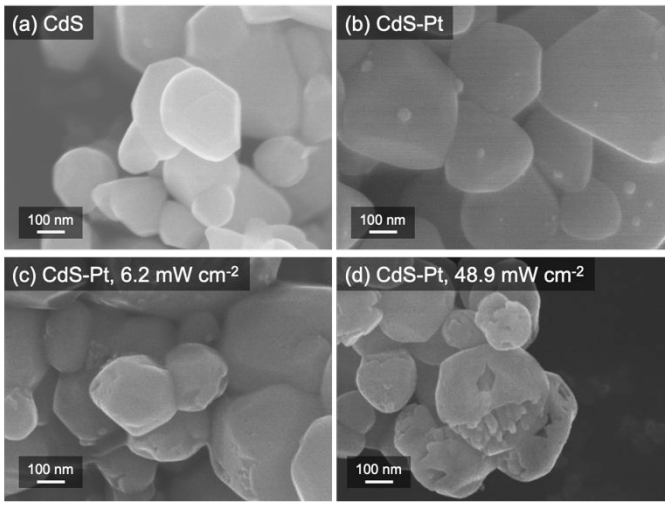


**Fig. 2** SEM images of (a) wurtzite CdS, (b) CdS-Pt prepared by the ETD method in the presence of 300 μmol $L^{-1}$ $[PtCl_6]^{2-}$ and 20 vol% lactic acid and CdS-Pt photoetched in the presence of 20 vol% lactic acid for 60 min under (c) 6.2 mW $cm^{-2}$ or (d) 48.9 mW $cm^{-2}$ visible light (430 nm).

initial "photoetching process" optimizes the particle morphology in view of quantum efficiency and stability.

First, zincblende CdS obtained via a liquid-phase method was annealed at 600 °C in a NaCl–$CaCl_2$ mixed molten salt to obtain highly crystalline particles.[10] Details of some experimental methods and processes of parameter optimization are provided in the Supplementary Information (SI). These are submicron-sized wurtzite CdS particles as indicated by XRD (Fig. S1a) and SEM (Fig. 2a) data. In addition, an absorption tailing characteristic of semiconductors with low crystallinity[11] observed for the precursor was clearly shortened due to the improved crystallinity (Fig. S1b). The wurtzite CdS thus obtained will be referred to simply as CdS hereafter.

The CdS particles (30 mg) were dispersed in an aqueous solution (5 mL), and loaded with Pt co-catalysts by an electron trap mediated deposition (ETD) method.[9,12] The particles were irradiated with light (430 nm, 48.9 mW $cm^{-2}$, LED) for 30 min in an aqueous solution containing 20 vol% lactic acid as an electron donor under $N_2$ or Ar atmosphere. As a result, electrons in the valence band are excited to the conduction band, and trapped by $S^{2-}$ defect sites, resulting in reduction of $Cd^{2+}$ at the CdS surface to metallic Cd. Then, $[PtCl_6]^{2-}$ was added to the dispersion (300 μmol $L^{-1}$) for galvanic replacement of Cd with Pt ($2Cd + Pt^{4+} \rightarrow Pt + 2Cd^{2+}$). The CdS photocatalyst thus modified with Pt nanoparticles is referred to as CdS-Pt. The typical SEM image showed that Pt nanoparticles with sizes of 5–20 nm were deposited on the CdS surface (Fig. 2b). In addition, signals for metallic Pt appeared in the Pt 4f region of the XPS spectrum (Fig. S2a).

Next, CdS-Pt particles were dispersed in a 20 vol% lactic acid aqueous solution and subjected to photoetching, in the course of photocatalytic hydrogen evolution at different light intensities. After light irradiation at 6.2 or 48.9 mW $cm^{-2}$ for 60 min, the particles were etched obviously as shown in SEM images (Fig. 2c,d). The etching was more extensive at the higher light intensity. The amounts of $Cd^{2+}$ dissolved from the CdS-Pt particles were determined by ICP-AES to be 3.2 and 15.1 mol% of Cd in the particles at the lower and higher light intensities, respectively. This trend qualitatively corresponds to the SEM results (Fig. 2c,d); etching of CdS was minimal at 6.2 mW $cm^{-2}$, and much more prominent at 48.9 mW $cm^{-2}$.

We also monitored the amount of hydrogen produced as a result of photocatalytic reduction of water during the light irradiation experiments. As shown in Fig. 3a,b, the hydrogen evolution rate was increased within 60 min. At 6.2 mW $cm^{-2}$, the evolution rate was 64 μmol $h^{-1}$ in the induction phase (0–15 min), and was increased to 75 μmol $h^{-1}$ after that (30–60 min). At 48.9 mW $cm^{-2}$, the initial rate was 266 μmol $h^{-1}$ (0–15 min), while the final rate at 30–60 min was 583 μmol $h^{-1}$. In the induction phase, the photoetching of CdS occurred, and the hydrogen evolution rate was improved. As CdS-Pt is etched and pores are formed, the volume of each CdS particle decreases, leading to a reduction in light absorption. However, if the particle concentration in the CdS suspension is sufficiently high to absorb all the incident photons, the EQE will not decrease. Rather, the distance for holes excited in the bulk to reach the CdS surface becomes shorter, leading to a decrease in recombination frequency, which results in an increase in both IQE and, consequently, EQE of the whole suspension.

To elucidate the changes in photocatalytic reactions during the photoetching process, the reaction products were quantitatively evaluated at 48.9 mW $cm^{-2}$ (Table 1, see SI for details). The production rates of hydrogen and pyruvic acid as the main product of lactic acid oxidation increased significantly after 30 min. In contrast, the amount of CdS dissolution significantly decreased after 30 min. These results indicate that photoetching proceeded to a certain extent and then it was

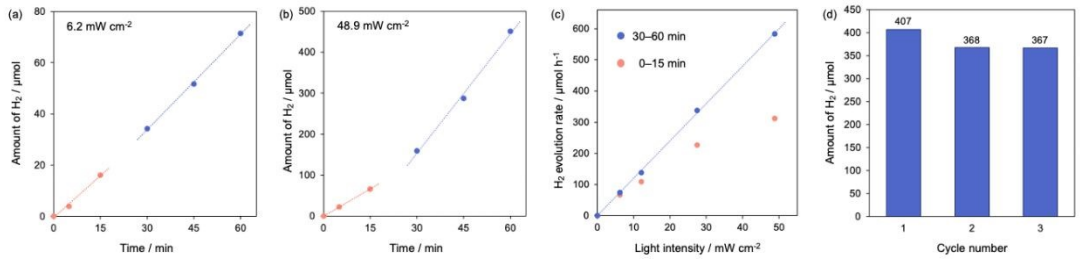


**Fig. 3** Time courses of the amount of evolved hydrogen gas for CdS-Pt (30 mg) particles suspended in a $N_2$-saturated aqueous solution (5 mL) containing 20 vol% lactic acid under visible light (λ = 430 nm) at (a) 6.2 mW $cm^{-2}$ and (b) 48.9 mW $cm^{-2}$. (c) Hydrogen evolution rates in the periods of 0–15 min and 30–60 min at different light intensities. (d) Cycling performance of photoetched CdS-Pt (3 mg) in 5 mL of 20 vol% lactic acid with strong light irradiation for 3 h each (365 nm, 1.0 W $cm^{-2}$).





 

suppressed, and made the lactic acid oxidation more dominant. A possible reason for the suppression of photocorrosion is the facet-selective etching of the CdS particles. According to previous reports, the wurtzite CdS(001) facet has a high surface energy and is unstable,[13] and photocorrosion preferentially proceeds on this facet in the presence of lactic acid.[9] In the present study, columnar structures were found after etching, suggesting that corrosion progressed along the [001] direction (Figs. 2d, S4). As a result, the unstable (001) facets were removed, while the corrosion-resistant (100) facets were left, so that the photocorrosion was suppressed.

Incidentally, the hydrogen evolution rate in the 30–60 min period increased linearly with the light intensity (Fig. 3c, $R^2 > 0.995$), indicating that the rate-determining step of the reaction is the photoexcitation process. Nevertheless, the overall reaction rate increased after the photocorrosion, likely because, as discussed above, the corrosion made it easier for photogenerated holes to reach the particle surface.

We also evaluated the turnover number of the present system. The CdS-Pt particles (3 mg) were dispersed in a 20 vol% lactic acid solution (5 mL), and irradiation with strong light for 3 h (365 nm, 1.0 W $cm^{-2}$) was repeated 3 times (Fig. 3d). The hydrogen evolution amount in the third cycle was almost the same as the second. In the overall 9 h process, the turnover number exceeded 50, indicating that the photocatalyst retained a sufficient stability without excess photoetching.

Next, the activity was evaluated in an aqueous solution containing 0.1 mol $L^{-1}$ $Na_2S$ and $Na_2SO_3$ as electron donors, instead of lactic acid. In the solution, $S^{2-}$ and $SO_3^{2-}$ ions suppress photocorrosion as good electron donors,[14] and the high pH value (~12) and $S^{2-}$ interfere with CdS dissolution. In fact, the photocorrosion was minimal, and the dissolution amount of CdS under 60 min of light irradiation was as low as 1.0 mol%. However, the hydrogen evolution rate saturated as the light intensity was increased, likely because the rate-limiting step has shifted from photoabsorption to redox reactions. We therefore examined the hydrogen evolution in the $Na_2S$-$Na_2SO_3$ solution after photoetching in a lactic acid solution under 48.9 mW $cm^{-2}$ light for 60 min. As a result, the evolution rate increased ~1.9 times (Fig. 4a). This should be due to the increase in the oxidation reaction rate by the morphological changes as mentioned above.

CdS photocatalysts are known to be stable in concentrated alkaline solutions, even without $Na_2S$, because replacement of $S^{2-}$ with $O^{2-}$ at the CdS surface protects CdS from photocorrosion.[15–17] In particular, in an alkaline solution containing isopropanol as an electron donor, a CdS-CdSe-Pt composite nanorod photocatalyst has achieved hydrogen evolution with an EQE of up to 99%,[18] due to the suppression of photocorrosion and use of $OH^-$ as an additional hole acceptor at the oxygenated or hydroxylated CdS surface.[19] It has also been reported that cadmium oxide can accept electrons excited in CdS and thereby promote charge separation.[20] On the basis of these insights, we investigated photocatalytic hydrogen production in a 1 mol $L^{-1}$ NaOH solution containing 20 vol% isopropanol by CdS-Pt and that photoetched in the lactic acid solution (Fig. 4b). As a result, the photoetching increased the hydrogen evolution rate by 5.6 times. XPS analysis of the sample after the reaction showed almost no change in the S 2p and Pt 4f spectra, whereas the Cd 3d peaks shifted to lower energies, reflecting the surface oxygenation or hydroxylation (Fig. S2). In addition, $Cd^{2+}$ was not detected by ICP-AES in the solution after the photocatalytic reaction for both of the CdS-Pt and photoetched CdS-Pt photocatalysts, indicating that those photocatalysts are sufficiently stable in the solution.

We also measured the EQE values for photocatalytic hydrogen evolution using the photoetched CdS-Pt photocatalyst under light irradiation at 430 nm. The EQE value was calculated from the amount of hydrogen produced between 60 and 90 min, during which a nearly constant production rate was observed. The obtained EQE value was 53.4 ± 1.7% in a 20 vol% lactic acid solution (Fig. 4c) and 86.1 ± 7.9% in 1 mol $L^{-1}$ NaOH solution containing 20 vol% isopropanol (Fig. 4d). Since the light transmittance into the solution in the test tube is lower than unity, the actual EQE value should be even higher. The highest EQE value reported for CdS-Pt photocatalysts has been ~60% (at 420 nm).[21] By utilizing the photoetching method, we exceeded this value and accomplished high EQE hydrogen evolution similar to that achieved by the CdS-CdSe-Pt composite nanorod photocatalysts by using a much simpler CdS-Pt system.

We also explored hydrogen production coupled with oxidative degradation of biomass, for potential application to practical photocatalytic systems. Here, 100 mg of α-cellulose (Wako, through 400 mesh (38 μm)) was dispersed as a biomass in a 10 mol $L^{-1}$ NaOH aqueous solution (5 mL) together with the present photoetched CdS-Pt photocatalyst. As a result, the EQE value reached 3.4 ± 0.7% up to 45 min of light irradiation, and 9.3 ± 1.2% after 60 min (Fig. 4e). In general, in the initial stage of the photocatalytic degradation of cellulose in an alkaline



**Table 1** The amounts of reductively evolved hydrogen, oxidatively generated pyruvic acid, acetic acid, formic acid, and dissolved CdS during the periods of 0–30 min and 0–60 min for CdS-Pt (30 mg) particles suspended in an Ar-saturated aqueous solution (5 mL) containing 20 vol% lactic acid under visible light (λ = 430 nm) at 48.9 mW $cm^{-2}$.

| Time / min | Hydrogen / μmol | Pyruvic acid / μmol | Acetic acid / μmol | Formic acid / μmol | Dissolved CdS / μmol |
|---|---|---|---|---|---|
| 30 | 178.8 | 94.1 | 10.7 | 6.9 | 29.6 |
| 60 | 420.6 | 303.2 | 17.4 | 10.7 | 31.5 |
| 60 (in dark) | 0.0 | 0.0 | 0.0 | 0.0 | 0.5 |

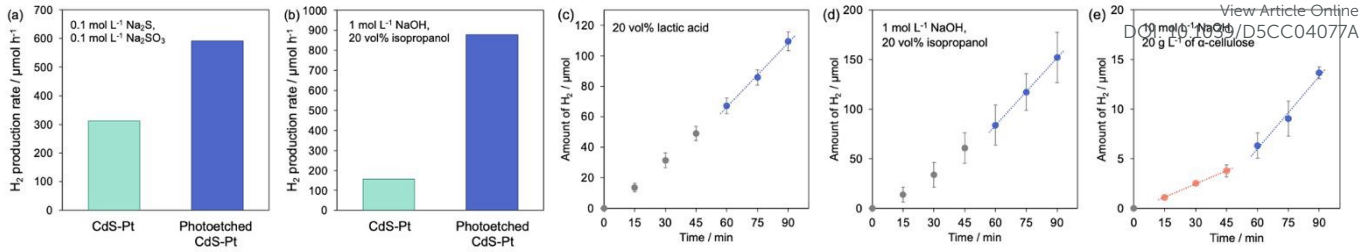


Fig. 4 Comparison of hydrogen evolution rates of CdS-Pt and photoetched CdS-Pt photocatalysts in (a) 0.1 mol $L^{-1}$ $Na_2S$, $Na_2SO_3$ and (b) 1 mol $L^{-1}$ NaOH, 20 vol% isopropanol. Time courses of the hydrogen evolution amount in (c) 20 vol% lactic acid, (d) 1 mol $L^{-1}$ NaOH, 20 vol% isopropanol and (e) 10 mol $L^{-1}$ NaOH, dispersed with 100 mg α-cellulose. Intensity of light (430 nm) was 48.9 mW $cm^{-2}$, and Irradiation area was 0.5 $cm^2$ for (a)–(c).

solution, a depolymerization of insoluble cellulose (*i.e.*, peeling process) is promoted by photocatalytic reactions.[22] While the hydrogen evolution rate is slow during this process, it is believed that once soluble low-molecular-weight products are formed, their oxidation becomes the main reaction, leading to an increase in the hydrogen evolution rate.[16] So far, the EQE value reported for hydrogen evolution with photoreforming of cellulose using CdS-based photocatalysts was 2.0% for the initial 60 min[23] and 2.95% for the initial 120 min (at 420 nm).[24] In the present study, the value for the initial 60 min was 4.0% at 430 nm, which was higher than the previously reported values. The value between 60 and 90 min was even higher, reaching 9.3%, indicating that photoetched CdS-Pt is highly suitable for hydrogen production coupled with cellulose photoreforming.

In summary, the morphology of the CdS-Pt photocatalyst was optimized in terms of photocatalytic activity and stability through photoetching based on the self-oxidation reaction. In particular, a high EQE value of 86.1 ± 7.9% was achieved in NaOH solution containing isopropanol as an electron donor. In addition, in the photoreforming of α-cellulose, an EQE value of 9.3 ± 1.2% was reached, exceeding the previously reported values. The present new method for enhancing the activity and stability of photocatalysts would be applied to various systems where photocorrosion can occur.

## Conflicts of interest

There are no conflicts to declare.

## Data availability

The data supporting this article have been included as part of the Supplementary Information.

## Notes and references

1 M. Grätzel, *Nature*, 2001, **414**, 338–344.
2 I. Tsuji, H. Kato, H. Kobayashi and A. Kudo, *J. Am. Chem. Soc.*, 2004, **126**, 13406–13413.
3 K. Sayama, K. Mukasa, R. Abe, Y. Abe and H. Arakawa, *Chem. Commun.*, 2001, 2416–2417.
4 G. Liu, H. G. Yang, J. Pan, Y. Q. Yang, G. Q. M. Lu and H. M. Cheng, *Chem. Rev.*, 2014, **114**, 9559–9612.
5 T. Takata, J. Jiang, Y. Sakata, M. Nakabayashi, N. Shibata, V. Nandal, K. Seki, T. Hisatomi and K. Domen, *Nature*, 2020, **581**, 411–414.
6 S. Ganesan, T. Kokulnathan, S. Sumathi and A. Palaniappan, *Sci. Rep.*, 2024, **14**, 2284.
7 X. Wang, Y. Xia, H. Wang, X. Jiao and D. Chen, *Chem. Commun.*, 2021, **57**, 4138–4141.
8 D. Meissner, C. Benndorf and R. Memming, *Appl. Surf. Sci.*, 1987, **27**, 423–436.
9 H. Nagakawa and T. Tatsuma, *J. Phys. Chem. C*, 2023, **127**, 20337–20343.
10 H. Nagakawa and T. Tatsuma, *ACS Appl. Energy Mater.*, 2022, **5**, 14652–14657.
11 B. Wang, G. M. Biesold, M. Zhang and Z. Lin, *Chem. Soc. Rev.*, 2021, **50**, 6914–6949.
12 T. Akiyama, H. Nagakawa and T. Tatsuma, *Phys. Chem. Chem. Phys.*, 2023, **25**, 9031–9035.
13 X. Jin, Y. Fang, T. Salim, M. Feng, Z. Yuan, S. Hadke, T. C. Sum and L. H. Wong, *Adv. Mater.*, 2021, **33**, 2104346.
14 A. Kudo and Y. Miseki, *Chem. Soc. Rev.*, 2009, **38**, 253–278.
15 D. W. Wakerley, M. F. Kuehnel, K. L. Orchard, K. H. Ly, T. E. Rosser and E. Reisner, *Nat. Energy*, 2017, **2**, 17021.
16 H. Nagakawa and M. Nagata, *ACS Appl. Mater. Interfaces*, 2021, **13**, 47511–47519.
17 H. Nagakawa, *Phys. Status Solidi A*, 2024, **221**, 2400213.
18 P. Kalisman, Y. Nakibli and L. Amirav, *Nano Lett.*, 2016, **16**, 1776–1781.
19 T. Simon, N. Bouchonville, M. J. Berr, A. Vaneski, A. Adrović, D. Volbers, R. Wyrwich, M. Döblinger, A. S. Susha, A. L. Rogach, F. Jäckel, J. K. Stolarczyk and J. Feldmann, *Nat. Mater.*, 2014, **13**, 1013–1018.
20 G. Wang, L. Gong, Z. Li, B. Wang, W. Zhang, B. Yuan, T. Zhou, X. Long and A. Kuang, *Phys. Chem. Chem. Phys.*, 2020, **22**, 9587–9592.
21 N. Bao, L. Shen, T. Takata and K. Domen, *Chem. Mater.*, 2008, **20**, 110–117.
22 V.-C. Nguyen, D. B. Nimbalkar, L. D. Nam, Y.-L. Lee and H. Teng, *ACS Catal.*, 2021, **11**, 4955–4967.
23 H. Nagakawa and M. Nagata, *ACS Appl. Energy Mater.*, 2021, **4**, 1059–1062.
24 S. Kamata, H. Nagakawa, A. Inaguma and M. Nagata, *ChemPhotoChem*, 2024, **8**, e202400018.

View Article Online
DOI: 10.1039/D5CC04077A

## Data availability

The data supporting this article have been included as part of the Supplementary Information.